Microwave Control of Atomic Motion in Optical Lattices

Leonid Förster, Michał Karski, Jai-Min Choi, Andreas Steffen, Wolfgang Alt, Dieter Meschede, and Artur Widera*
Institut für Angewandte Physik, Universität Bonn, Wegelerstrasse 8, D-53115 Bonn, Germany

Enrique Montano, Jae Hoon Lee, Worawarong Rakreungdet, and Poul S. Jessen
CQuIC, College of Optical Sciences, University of Arizona, Tucson, Arizona 85721, USA
(Received 3 September 2009; published 3 December 2009)

We control the quantum mechanical motion of neutral atoms in an optical lattice by driving microwave transitions between spin states whose trapping potentials are spatially offset. Control of this offset with nanometer precision allows for adjustment of the coupling strength between different motional states, analogous to an adjustable effective Lamb-Dicke factor. This is used both for efficient one-dimensional sideband cooling of individual atoms to a vibrational ground state population of 97% and to drive coherent Rabi oscillation between arbitrary pairs of vibrational states. We further show that microwaves can drive well resolved transitions between motional states in maximally offset, shallow lattices, and thus in principle allow for coherent control of long-range quantum transport.

DOI: 10.1103/PhysRevLett.103.233001 PACS numbers: 37.10.Jk, 05.60.Gg, 37.10.De, 37.10.Vz

Accurate, simultaneous control of multiple degrees of freedom is crucial for the experimental realization of quantum information processing and quantum simulation [1]. Thus, in schemes that use trapped ions or atoms as carriers of quantum information, qubits are often encoded in internal states and the motional degree of freedom is manipulated to engineer state-dependent interactions between them. In ion traps this involves the controlled excitation of a collective mode of vibration [2], leading to robust quantum gate protocols and entanglement of multiple qubits [3]. Proposals based on neutral atoms in optical lattices rely instead on short-range collisional interactions that occur only when the center-of-mass wave packets overlap [4]. Accurate control of the collisional interaction thus requires preparation of pure center-of-mass states, and the ability to move atoms conditionally on the qubit state. Variations of this approach have been used to entangle pairs [5] and chains of atoms [6], with a fidelity limited mainly by the speed and accuracy with which the optical potentials can be changed during the transport phase. For this reason there has been considerable interest in optimal control techniques to improve atom transport in optical lattices and other traps [7], mostly through more elaborate control of the trapping potentials. Here we show that microwave coupling between spatially offset, state-dependent lattices allows sideband cooling to the vibrational ground state, and thus offers an alternative means for wave packet initialization in lattice geometries that cannot easily be loaded from a Bose-Einstein condensate [8,9]. Our approach also provides new tools for coherent control of atomic motion in static potentials [10]. In principle this enables the generation of a broad class of spin-motion entangled states [11,12], and lends itself to the application of composite pulses and other robust control techniques (see Ref. [13] and references therein).

We consider caesium (Cs) atoms with two hyperfine states $|\downarrow\rangle \equiv |F = 3, m_F = 3\rangle$ and $|\uparrow\rangle \equiv |F = 4, m_F = 4\rangle$, which are coupled by microwave radiation. Here F and m_F are the total angular momentum and its projection onto the quantization axis, respectively. Microwaves provide a coherent, homogeneous and readily controllable radiation field, but since microwave photons have negligible momentum they are rarely considered for driving transitions between vibrational states in atom and ion traps. We circumvent this limitation by trapping atoms in the $|\downarrow\rangle$ and $|\uparrow\rangle$ states in separate optical lattice potentials offset by a distance Δx. The matrix element for a vibrational transition is then proportional to the center-of-mass wave function overlap, i.e., the Franck-Condon factor,

$$\hbar\,\Omega_{n,n'} = \hbar\Omega_0\langle\tilde{n}'|e^{-i\Delta x\hat{p}/\hbar}|\tilde{n}\rangle = \hbar\Omega_0\langle n'|n\rangle, \qquad (1)$$

where Ω_0 is the "bare" Rabi frequency for the $|\downarrow\rangle$ to $|\uparrow\rangle$ transition in free space, n' and n ($\tilde{n}'$ and $\tilde{n}$) label the vibrational quantum states in the shifted (unshifted) $|\downarrow\rangle$ and $|\uparrow\rangle$ potentials, and $\hat{p}$ is the momentum operator. From Eq. (1) an effective Lamb-Dicke parameter $\eta_{\mathrm{eff}} \equiv i\Delta x p_0/\hbar$ can be defined, where p_0 is the size of the harmonic oscillator ground state in momentum space. In analogy to the usual Lamb-Dicke parameter defined for optical transitions in traps with no offset, η_{eff} enters as a common factor in the Franck-Condon factors for various n, n' [14]. Changing Δx allows us to tune the Franck-Condon factor (and thus $\Omega_{n,n'}$) between an arbitrary pair of vibrational states from zero to $\sim$0.5.

Comparing the size of the ground state wave packet x_0 with the lattice spacing a_{lat}, one can identify two regimes where the physics is qualitatively different. For deep lattices the atomic wave packets are strongly localized, and the overlap between different vibrational states is only significant for displacements $\Delta x \ll a_{\mathrm{lat}}$. In this situation

the motion is confined to a pair of neighboring wells of the $|\downarrow\rangle$ and $|\uparrow\rangle$ lattices; see Figs. 1(a) and 1(b). This regime is similar to the recently reported coupling of a charge-phase qubit to an LC oscillator [15] or the coupling of motional and spin states of trapped ions using rf radiation and a static magnetic field [14].

For shallow lattices the extent of the wave packet becomes comparable to half the lattice spacing ($x_0 \lesssim a_{\mathrm{lat}}/2$). In this regime the overlap between the $|\downarrow\rangle$ and $|\uparrow\rangle$ wave packets is significant even for the maximum offset of $\Delta x = a_{\mathrm{lat}}/2$. In that case the microwave field introduces nearest-neighbor coupling between potential wells throughout the $|\downarrow\rangle$ and $|\uparrow\rangle$ lattices as illustrated in Figs. 1(c) and 1(d). The result is a quantum walk of the atom on the lattice [9], equivalent to ballistic tunneling in a $\lambda_{\mathrm{lat}}/4$ period microwave dressed lattice potential.

Our lattices are created by two counterpropagating laser beams with linear polarizations forming an angle ϑ. The resulting light field consists of two circularly polarized standing waves, which can be shifted in opposite directions along the axis by adjusting the angle ϑ. Because of the different tensor polarizabilities of the $|\downarrow\rangle$ and $|\uparrow\rangle$ states, this leads to spatial offset of their respective lattice potentials [16]. Microwave radiation around 9.2 GHz couples the $|\downarrow\rangle$ and $|\uparrow\rangle$ states with a bare Rabi frequency Ω_0 of up to 60 kHz, while a magnetic field of up to 3 G lifts their degeneracy with other Zeeman states. Spectra are obtained by scanning the frequency of the microwave field and detecting the number of atoms in state $|\downarrow\rangle$ or state $|\uparrow\rangle$ [13,17]. For $\Delta x = 0$, transitions to different vibrational levels are not detectable, but when the displacement is sufficient for the effective Lamb-Dicke parameter η_{eff} to be non-negligible, the spectrum consists of both a carrier ($|\uparrow, n\rangle \leftrightarrow |\downarrow, n\rangle$ transitions) and sidebands at $\pm\omega_{\mathrm{ax}}$ ($|\uparrow, n\rangle \leftrightarrow |\downarrow, n \pm 1\rangle$ transitions); see Fig. 2.

The regimes of strong and weak confinement have been realized in separate experiments [18]. Strong confinement is realized in a one-dimensional (1D) geometry, in which two counterpropagating laser beams with a wavelength of $\lambda_{\mathrm{lat}} = 865.9$ nm are focused to a waist of 20 μm. After molasses cooling and subsequent adiabatic lowering of the trap depth to $k_B \times 80$ μK, the atoms have a typical temperature of ~ 10 μK. For our axial and radial trapping frequencies of $\omega_{\mathrm{ax}} = 2\pi \times 110$ kHz and $\omega_{\mathrm{rad}} \approx 2\pi \times 1.1$ kHz, the atoms populate vibrational states with a mean quantum number of $\bar{n} \approx 1.2$ axially and $\bar{n}_{\mathrm{rad}} \approx 200$ radially.

Weak confinement is realized in a shallow, three-dimensional optical lattice consisting of three individual 1D lattices whose optical frequencies differ by tens of MHz. The lattice is loaded with 10^6 Cs atoms, which are sideband cooled [19] into the $|\downarrow\rangle$ state, with a mean vibrational excitation of 0.1–0.2 for each dimension. During microwave spectroscopy we set $\vartheta = 0$ for the transverse lattices, and the lattice depths are adjusted to obtain vibrational frequencies $\omega_{\mathrm{ax}} = \omega_{\mathrm{trans}} = 2\pi \times 18$ kHz. The common lattice detuning is 140 GHz blue of the Cs D_2 line, where the $|\downarrow, 0\rangle \leftrightarrow |\uparrow, \{0, 1\}\rangle$ transition frequencies show minimal dependence on lattice depth; see below.

In the strongly confining lattice we begin our experiments by sideband cooling the atoms with a microwave field tuned to the $|\uparrow, n\rangle \leftrightarrow |\downarrow, n-1\rangle$ transitions. This corresponds to the blue sideband of the spectrum as the cooling cycle starts in the upper hyperfine state. Repumping on the $F = 3 \rightarrow F' = 4$ transition of the D_2

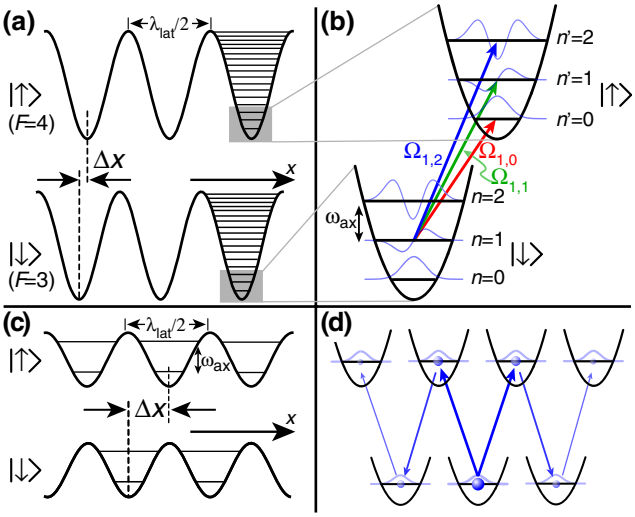

FIG. 1 (color online). (a) Deep, slightly offset state-dependent optical lattices for the $|\downarrow\rangle$ and $|\uparrow\rangle$ hyperfine states. (b) The offset enables on site microwave transitions changing the vibrational quantum number. (c) Maximally offset, shallow lattices. (d) Microwave radiation can couple an initially localized population of $|\downarrow\rangle$ symmetrically to the neighboring potential wells and further throughout the lattice.

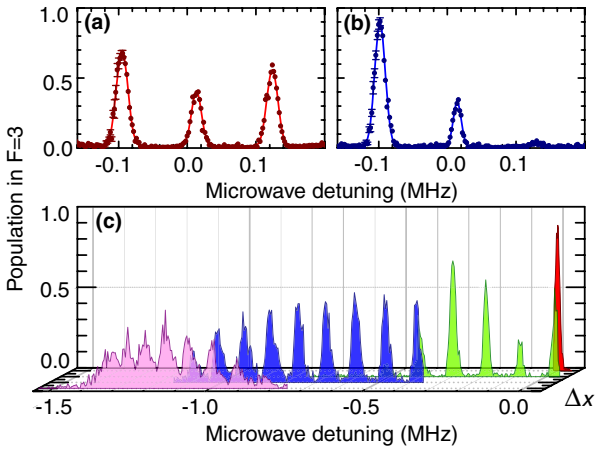

FIG. 2 (color online). Microwave spectra for strong confining and slightly displaced ($\Delta x = 24$ nm, $\vartheta = 0.064\pi$) traps, for (a) molasses cooled and (b) sideband cooled atoms with a ground state population of 97%. The pulse area amounts to π for both sidebands and to 1.6π for the carrier. (c) Spectrum for all vibrational states in the trap, starting from the axial ground state. The different spectra correspond to (from back to front) $\Delta x = \{0, 43, 111, 176\}$ nm ($\vartheta = \{0, 0.112, 0.280, 0.420\}\pi$).

line breaks the coherence of the microwave transition, and subsequent spontaneous emission brings the atom back to the $|\uparrow\rangle$ state. In addition, a second, circularly polarized laser beam on the $F = 4 \rightarrow F' = 4$ transition ensures spin polarization in state $|\uparrow\rangle$. We apply the microwave field and repumping laser simultaneously for 20 ms. For the repumping process, both the recoil of the photon and the lattice shift violate the assumption of a preserved vibrational quantum number [20]. The influence of the latter is minimized by choosing a relatively small lattice angle for cooling ($\vartheta = 0.025\pi$, $\Delta x = 10$ nm). A spectrum of sideband cooled atoms is shown in Fig. 2(b). By comparing the areas of the blue and red sideband peaks [21] we find 97% axial ground state population ($\bar{n} = 0.03 \pm 0.01$, $T_{\mathrm{ax}} = (1.6 \pm 0.1)\ \mu$K), mainly limited by residual off-resonant excitation of the final state.

Vibrational spectra can be obtained by adjusting the coupling strength to favor transitions from the axial ground state to a chosen group of final states. Figure 2(c) shows a series of four such spectra measured for different Δx, mapping out all bound states in our trap. The experimentally measured transition frequencies are in agreement with a 1D band structure calculation, but the observed linewidths suffer from inhomogeneous broadening associated with the (uncooled) radial motion of the atoms. Because of the nonharmonic radial potential the transition frequency depends on both the radial position and the order of the sideband [20].

Coherent Rabi oscillations for the first and seventh red sideband transitions starting from state $|\uparrow, 0\rangle$ are shown in Figs. 3(a) and 3(b). Their Rabi frequencies can be adjusted by the displacement Δx to be on the same order of magnitude as the bare Rabi frequency of 60 kHz. It is also instructive to observe Rabi oscillations that start from a thermal distribution of vibrational states. In that case the signal is a sum of Rabi oscillations at a series of distinct frequencies, each corresponding to a transition $|\uparrow, n\rangle \leftrightarrow |\downarrow, n\rangle$ and contributing in proportion to the population of the initial state. Figure 3(c) shows such a beat signal obtained for $\Delta x = 15$ nm ($\vartheta = 0.036\pi$). From the Fourier transform [Fig. 3(d)] we deduce the probability of occupancy $p(n) \sim \exp[-E_n/(k_B T)]$ [22]. This leads to a mean axial vibrational quantum number of $\bar{n} = 1.0 \pm 0.2$ [$T_{\mathrm{ax}} = (8 \pm 1)\ \mu$K].

To illustrate the range of adjustable coupling strength, we measure the Rabi frequencies of three transitions (the carrier and the first red and blue sidebands) starting from the $|\downarrow, 1\rangle$ state for different displacements Δx; see Fig. 4. For weak coupling ($\Omega_0/\omega_{\mathrm{ax}} \ll 1$), this yields direct information on the wave function overlap between the initial and final wave functions according to Eq. (1). Since our data are not taken in this regime, we compare instead to a theoretical model that takes into account microwave dressing and off-resonance excitation. This is done by first calculating the band structure and Bloch states [23], then integrating the Schrödinger equation in the Bloch basis, and finally determining the Rabi frequency from the time dependent oscillation of the $|\downarrow\rangle$ and $|\uparrow\rangle$ states. Transverse motion in strongly confined lattices is modeled by averaging the result of several such calculations for different lattice depths. For most displacements, our model predictions differ negligibly from Eq. (1), and reproduce our experimental data for strong and weak confinement quite well.

In our weakly confining lattice a small but nonzero Rabi frequency remains even for displacements of $\Delta x = \lambda_{\mathrm{lat}}/4$, as shown in the inset in Fig. 4. We stress that in a 3D lattice, spatial inhomogeneities of the trapping potential can lead to frequency broadening of transitions between the various bound states, but that it is possible to find a "magic" lattice

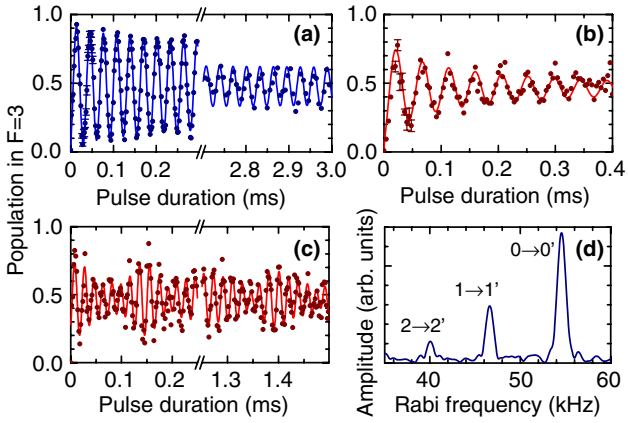

FIG. 3 (color online). Rabi oscillations for the $|\uparrow, 0\rangle \leftrightarrow |\downarrow, 1\rangle$ (a) and $|\uparrow, 0\rangle \leftrightarrow |\downarrow, 7\rangle$ (b) transitions with Rabi frequencies of $2\pi \times 32$ kHz and $2\pi \times 22$ kHz. Solid lines are sines damped by the empirically found function $\exp(-\sqrt{t/\tau})$ to account for radial dynamics. We find $\tau_{(a)} = (2.0 \pm 0.1)$ ms, $\tau_{(b)} = (90 \pm 10)\ \mu$s. (c) Rabi oscillations on the carrier for a thermal initial state and (d) its Fourier transform. From the amplitudes we deduce $T_{\mathrm{ax}} = (8 \pm 1)\ \mu$K.

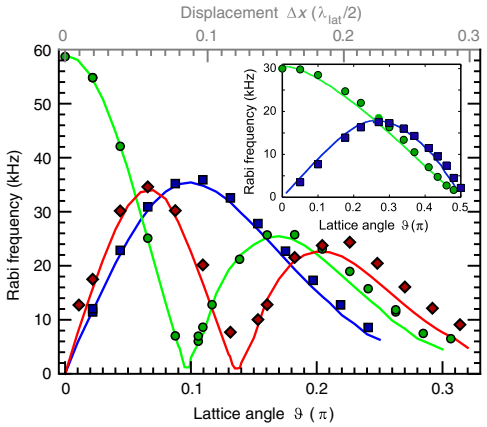

FIG. 4 (color online). Measured Rabi frequencies of the carrier (○) and the red (◇) and blue (□) sidebands, starting from state $|\downarrow, 1\rangle$ for different polarization angles ϑ. Solid lines are predictions of a full model. The offset Δx (upper axis) depends nonlinearly on the polarization angle ϑ. The inset shows measured and calculated Rabi frequencies in a shallow lattice, for $\vartheta \leq \pi/2$.

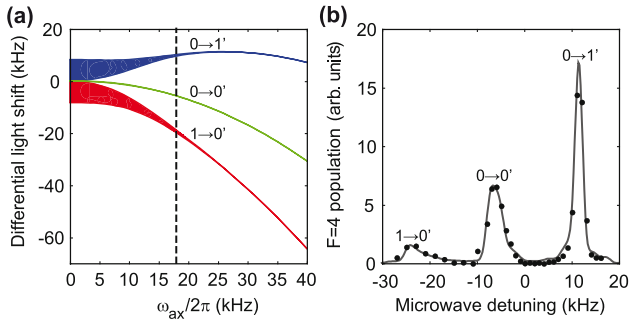

FIG. 5 (color online). Vibrational spectroscopy in a weakly confining lattice with $\Delta x = \lambda_{\mathrm{lat}}/4$. (a) Calculated light shift of the $|\downarrow, 0\rangle \leftrightarrow |\uparrow, \{0, 1\}\rangle$ carrier and sideband transitions. The shaded areas indicate line broadening due to band curvature. The dashed line indicates the ω_{ax} used in our experiment. (b) Microwave spectrum. Solid points are experimental data, the line a prediction from our full model. The various linewidths reflect the slope of the light shift curves in (a).

detuning [24] for which this sensitivity is suppressed for some states and for a limited range of ω_{ax} [Fig. 5(a)]. Figure 5(b) shows an example of a measured spectrum in a lattice with $\Delta x = \lambda_{\mathrm{lat}}/4$, along with a theoretical prediction from our model based on integrating the Schrödinger equation in the Bloch basis and including inhomogeneous broadening from variations in the lattice depth and magnetic field across the atomic ensemble. The excitation pulse has a Gaussian envelope with a 1 ms full width at half maximum and pulse areas of 0.35π for the $|\downarrow, 0\rangle \leftrightarrow |\uparrow, 0\rangle$ transition and 0.9π for the $|\downarrow, 0\rangle \leftrightarrow |\uparrow, 1\rangle$ transition. In this geometry, coupling between states throughout the lattice [Figs. 1(c) and 1(d)] will drive a quantum walk that delocalizes an atom in space on a time scale comparable to the Rabi period. At this point tracing over the spatial degree of freedom leads to a statistical mixture of the $|\downarrow\rangle$ and $|\uparrow\rangle$ states. Experimentally, we see this as a rapid damping of the Rabi oscillation. The demonstration of clearly resolvable lines in the microwave spectrum is a prerequisite for control of quantum transport, explored theoretically in [12].

In summary, we have demonstrated microwave control of atomic motion in state-dependent optical lattices. We have used this to implement a convenient scheme for sideband cooling, and to drive coherent Rabi oscillations between selected pairs of vibrational states. In the near term our approach may prove useful in optical lattice based quantum simulation, e.g., by populating high-lying bands and controlling the tunneling properties in deep lattice potentials. Possible applications include investigations of nonequilibrium systems [25] on the border between classical and quantum thermodynamics. Other prospects include detection and control of two-body interactions and trap induced resonances [26]. In the longer term, microwave driven quantum transport may be a good candidate for robust control, which will likely prove essential to quantum information processing.

We acknowledge financial support by DFG (research unit 635), the EU (IP SCALA), the NSF (PHY-0555673), and IARPA (DAAD19-13-R-0011). M. K. acknowledges support by Studienstiftung des deutschen Volkes, J. M. C. from the Korean Government (MOEHRD).

*widera@uni-bonn.de

[1] M. A. Nielsen and I. L. Chuang, *Quantum Computation and Quantum Information* (Cambridge University Press, Cambridge, England, 2000).
[2] J. I. Cirac and P. Zoller, Phys. Rev. Lett. **74**, 4091 (1995); C. Monroe, D. M. Meekhof, B. E. King, W. M. Itano, and D. J. Wineland, Phys. Rev. Lett. **75**, 4714 (1995).
[3] D. Leibfried *et al.*, Nature (London) **438**, 639 (2005); H. Haffner *et al.*, Nature (London) **438**, 643 (2005).
[4] D. Jaksch, H. Briegel, J. I. Cirac, C. W. Gardiner, and P. Zoller, Phys. Rev. Lett. **82**, 1975 (1999); G. K. Brennen, C. M. Caves, P. S. Jessen, and I. H. Deutsch, Phys. Rev. Lett. **82**, 1060 (1999).
[5] M. Anderlini *et al.*, Nature (London) **448**, 452 (2007).
[6] O. Mandel *et al.*, Nature (London) **425**, 937 (2003).
[7] T. Calarco *et al.*, Phys. Rev. A **61**, 022304 (2000); C. E. Creffield, Phys. Rev. Lett. **99**, 110501 (2007); W. Merkel *et al.*, Phys. Rev. A **75**, 033420 (2007); G. D. Chiara *et al.*, Phys. Rev. A **77**, 052333 (2008).
[8] K. D. Nelson, X. Li, and D. S. Weiss, Nature Phys. **3**, 556 (2007).
[9] M. Karski *et al.*, Science **325**, 174 (2009).
[10] A. B. Deb, G. Smirne, R. M. Godun, and C. J. Foot, J. Phys. B **40**, 4131 (2007).
[11] H. L. Haroutyunyan and G. Nienhuis, Phys. Rev. A **64**, 033424 (2001).
[12] B. E. Mischuck, P. S. Jessen, and I. H. Deutsch, arxiv: 0905.1094.
[13] W. Rakreungdet *et al.*, Phys. Rev. A **79**, 022316 (2009).
[14] M. Johanning *et al.*, Phys. Rev. Lett. **102**, 073004 (2009).
[15] D. Gunnarsson *et al.*, Phys. Rev. Lett. **101**, 256806 (2008).
[16] O. Mandel *et al.*, Phys. Rev. Lett. **91**, 010407 (2003).
[17] S. Kuhr *et al.*, Phys. Rev. Lett. **91** 213002 (2003).
[18] Experiments with strongly confining lattices were done at the Universität Bonn, those with shallow lattices at the University of Arizona.
[19] S. E. Hamann *et al.*, Phys. Rev. Lett. **80**, 4149 (1998).
[20] Details will be presented in an upcoming publication.
[21] F. Diedrich, J. C. Bergquist, W. M. Itano, and D. J. Wineland, Phys. Rev. Lett. **62**, 403 (1989).
[22] D. M. Meekhof, C. Monroe, B. E. King, W. M. Itano, and D. J. Wineland, Phys. Rev. Lett. **76**, 1796 (1996).
[23] P. S. Jessen and I. H. Deutsch, Adv. At. Mol. Opt. Phys. **37**, 95 (1996).
[24] H. Katori, M. Takamoto, V. G. Pal'chikov, and V. D. Ovsiannikov, Phys. Rev. Lett. **91**, 173005 (2003).
[25] C. Jarzynski, Phys. Rev. Lett. **78**, 2690 (1997).
[26] R. Stock, I. H. Deutsch, and E. L. Bolda, Phys. Rev. Lett. **91**, 183201 (2003).